Available online at www.sciencedirect.com
ScienceDirect
Trans. Nonferrous Met. Soc. China 30(2020) 3263−3273
Transactions of Nonferrous Metals Society of China
www.tnmsc.cn

Influence of multipass high rotating speed friction stir processing on microstructure evolution, corrosion behavior and mechanical properties of stirred zone on AZ31 alloy

Fen-jun LIU[1,2], Yan JI[1,2], Yan-xia BAI[1]

1. College of Energy Engineering, Yulin University, Yulin 719000, China;
2. Yulin Key Laboratory of Metal Matrix Composites and Remanufacturing Technology, Yulin University, Yulin 719000, China

Received 1 March 2020; accepted 4 September 2020

Abstract: The influence of multipass high rotating speed friction stir processing (FSP) on the microstructure evolution, corrosion behavior, and tensile properties of the stirred zone (SZ) was investigated by EBSD, TEM, SEM, electrochemical workstation and electronic universal testing machine. The mean grain size of the SZ is significantly refined, and it increases with the increase of the processing pass. In addition to an obvious increase in the number, the distribution of β-$Al_{12}Mg_{17}$ precipitates also becomes more uniform and dispersed with increasing the processing pass. Compared with the as-received AZ31 alloy, the tensile properties of the SZ are hardly improved, but the corrosion resistances are significantly enhanced. The corrosion potential of the SZ prepared by 4-pass FSP is increased from −1.56 V for the unprocessed AZ31 alloy to −1.19 V, while the corrosion current is decreased from 1.55×10^{-4} to 5.47×10^{-5} A.

Key words: AZ31 alloy; high rotating speed; multipass friction stir processing; microstructure evolution; corrosion resistance; mechanical properties

1 Introduction

Magnesium alloys are widely considered to be one of the most environmentally friendly structural materials for achieving lightweight design and energy saving in the applications of transportation industries due to their high specific strength, low density, and abundant deposits [1,2]. However, poor corrosion resistance and limited tensile properties have severely restricted the further application of magnesium alloys [3,4]. Grain refinement is considered to be an effective method to enhance the corrosion resistance and tensile properties of magnesium alloys [5−8]. It is urgent to develop a method suitable for grain refinement of magnesium alloys. Severe plastic deformation can significantly make the grain refined, such as friction stir processing (FSP) [9−11]. FSP derived from friction stir welding is a promising severe plastic deformation technique to change the microstructure, especially in grain refinement and microstructure homogenization.

Multipass high rotating speed FSP is a novel severe plastic deformation technique based on multipass conventional rotating speed FSP. Compared with multipass conventional rotating speed FSP, the most obvious technical feature of multipass high rotating speed FSP is that the rotating speed of the pin tool is significantly higher.

Foundation item: Projects (51861034, 51601167) supported by the National Natural Science Foundation of China; Project (2020GY-262) supported by the Science and Technology Department of Shaanxi Province, China; Project (2019-86-1) supported by the Technology Bureau of Yulin, China; Project (20GK06) supported by the High-level Talent Program of Yulin University, China

Corresponding author: Fen-jun LIU; Tel: +86-912-3891273; E-mail: lfjxcmg@126.com

DOI: 10.1016/S1003-6326(20)65459-0

Multipass conventional rotating speed FSP has been greatly developed in improving the surface corrosion resistance and tensile properties of the Mg−Al−Zn series alloys by refining grain size and homogenizing the microstructure [12,13]. CHAI et al [14] processed an as-cast AZ91D alloy plate using multipass FSP at 800 r/min and found that the mechanical properties of the processed AZ91D alloy were enhanced to some extent due to the strengthening of fine grain and solution and dispersion of β-$Al_{12}Mg_{17}$ phase. LUO et al [15] have done multipass FSP at 1000 r/min on an as-cast AZ61 alloy plate and produced an obvious grain refinement in the stirred zone (SZ) without macrodefects. An effective enhancement in the tensile properties of the processed AZ61 alloy plate is obtained due to the elimination of cast defects and the formation of refined grains. A similar work was also performed on an as-cast AZ61 alloy plate using multipass submerged FSP at 800 r/min and it was found that the mean grain size prepared in the SZ is 2.0−5.4 μm [16]. A significant enhancement in tensile properties of the processed AZ61 alloy plate is exhibited attributed to the strengthening of dislocation, solution and grain refinement. VENKATESWARLU et al [17] applied multipass FSP on an AZ31B alloy plate at 1150 r/min with overlapping of 1, resulting in an enhancement in mechanical properties due to the formation of equiaxed homogeneous and refined microstructure in the stirred zone (SZ). NIA et al [18] also investigated the mechanical properties of the processed AZ31 alloy plate prepared using multipass FSP at 1000 r/min with a 50% overlap and rapid cooling and found that FSP with different processing directions can obviously refine the grains size, homogenize the grain distribution in SZ and increase the microhardness and tensile properties. LIU et al [19] applied multipass FSP on an as-cast AZ31 alloy plate at 1000 r/min with a 100% overlap, resulting in an enhancement in microhardness and corrosion resistance in the subsequent passes due to the significant grain refinement in the SZ. Although multipass conventional FSP can significantly improve corrosion performance and tensile properties of the Mg−Al−Zn series alloys by changing the microstructure characteristics, the rotating speed of pin tool used for the FSP is mostly based on the conventional rotating speed, that is, the rotating speed of the pin tool is generally less than 2000 r/min [20]. Moreover, according to the authors' knowledge, there are few public reports on the application of multi-pass high rotating speed FSP to improve the corrosion resistance and mechanical properties of AZ31 alloy.

The main purpose in the current work was to prepare AZ31 alloy plate with excellent corrosion resistance and tensile properties using multipass high rotating speed FSP. In addition to discussing the relationship between inhomogeneous microstructure and tensile properties, the effects of subsequent passes on microstructure characteristics, corrosion resistance, microhardness and tensile properties of the high rotating speed friction stir processed AZ31 alloy plate are discussed and analyzed.

2 Experimental

2.1 Material and FSP

The AZ31 alloy (3Al−1Zn−Mg, wt.%) of 2 mm-thick hot-squeezed plate was applied in the present work. Prior to FSP, the workpieces with the dimensions of 150 mm in length and 100 mm in width were machined from the as-squeezed AZ31 alloy plate as the base metal (BM) for FSP using a wire electrical discharge machining. The BM was subjected to 1-pass, 2-pass and 4-pass FSP, respectively. FSP was carried out using FSW-TS-F08-DZ high-speed welding equipment at 3000 r/min and 75 mm/min. The pin tool with a three-helix concave shoulder of 12 mm in diameter and a conical probe of 1.5 mm in length, 2 mm and 3 mm in diameter at top and root was employed in the present FSP. The plunge depth of tool shoulder and the tilt angle of pin tool were fixed at 0.2 mm and 0°, respectively. In the FSP process, the proceeding direction was parallel to the hot squeezing direction, and subsequent processing path completely coincided with the previous one. In other words, the travel path of the pin tool is the same as the previous one with a 100% overlap. The processed AZ31 alloy plate specimens prepared by multipass high rotating speed FSP are labeled in abbreviated form. For example, the 3000-75-4 sample denotes the processed AZ31 alloy plate was produced using four-pass FSP at 3000 r/min and 75 mm/min.

2.2 Microanalysis

The microstructure observations were conducted on the BM and SZ of the processed AZ31 alloy plate using SEM (TESCAN MIRA3 XMU) along with an EBSD detector (OXFORD NORDALYS DETECTOR) and TEM (FEI TECANI-F30). For EBSD observation, the samples were cross-sectioned perpendicular to the hot-squeezed direction and processing direction, respectively, prepared by a standard metallographic method and then electrolytically polished with a solution of 50 mL perchloric acid and 950 mL ethanol. The EBSD results were analyzed using the HKL-Channel 5 software. For TEM observation, the thin foils of the SZ machined parallel to the processing direction were punched using twin-jet electro-polishing method at 248 K in a solution of perchloric acid (25 mL) and ethanol (475 mL). Schematic diagrams of sampling position and test position for EBSD and TEM observation samples are shown in Fig. 1.

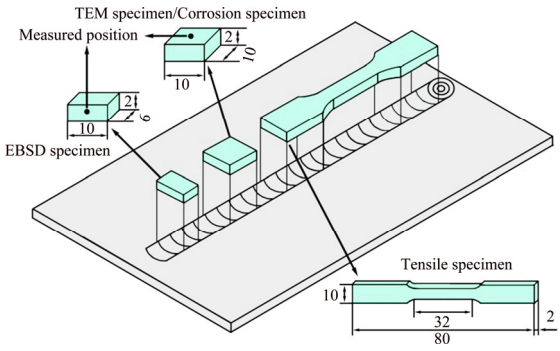

Fig. 1 Schematic diagrams of sampling position and measured specimen (Unit: mm)

2.3 Corrosion and mechanical properties tests

In order to assess the corrosion resistance and mechanical properties of the processed AZ31 alloy plate, a typical three-electrode cell system (VERSASTAT 400), Vickers microhardness tester (HMV-1) and electronic universal testing machine (INSTRON 3382) were employed to test the potentiodynamic polarization curve, electro-chemical impedance spectroscopy, microhardness distribution, and room temperature tensile properties. The SZ and BM were cut into square specimens having a side length of 10 mm for corrosion resistance testing. The specimens of the SZ and BM, an Ag/AgCl electrode and a square platinum foil of 10 mm in length were taken as working electrode, reference electrode and auxiliary electrode, respectively. Microhardness distributions along the transverse cross section centerline of the SZ were measured using a step size of 0.25 mm at 100 g load for 10 s. Tensile testing was performed at room temperature using the speed of 1 mm/min. The corrosion failure mechanism and tensile fracture behavior of the BM and SZ were investigated using SEM. The sampling position and main dimensions of the tensile specimen are shown in Fig. 1.

3 Results and discussion

3.1 Microstructure evolution

The microstructure characteristics of the BM perpendicular to the hot-squeezed direction are exhibited in Figs. 2(a−d). It can be seen that the BM consists of equiaxed grains and massive high angle grain boundaries (HAGBs). The mean grain size of 11.6 μm is ascertained using the linear intercept method. In addition, a large number of small β-$Al_{12}Mg_{17}$ precipitates are distributed in the BM, as shown in Fig. 3(a). The β-$Al_{12}Mg_{17}$ precipitates distribute inhomogeneously and agglomerate in some areas. According to the first principle calculation results, the stacking fault energy (SFE) of magnesium alloys is decreased with increasing the content of aluminum [21]. That is to say, magnesium alloy with high aluminum content has a beneficial effect on the formation of fine grain microstructure during hot deformation. The BM is subjected to the severe hot extrusion deformation during hot squeezing, which results in a relatively fine equiaxed grain structure in the BM. In the subsequent cooling stage, partial subgrain boundaries and high density dislocation walls convert into the HAGBs, and eventually a large number of HAGBs and relatively small misorientation angle are produced in the BM, as shown in Figs. 2(b, d). Moreover, the growth and diffusion of the β-$Al_{12}Mg_{17}$ precipitates are also inhibited during the cooling stage, resulting in a large number of small precipitates and their inhomogeneous distributions in the BM.

The microstructures of the SZ perpendicular to the FSP direction including the grain morphology, grain boundary, distribution of grain size and misorientation angle, and precipitate characteristic are presented in Figs. 2−4. The equiaxed grains in

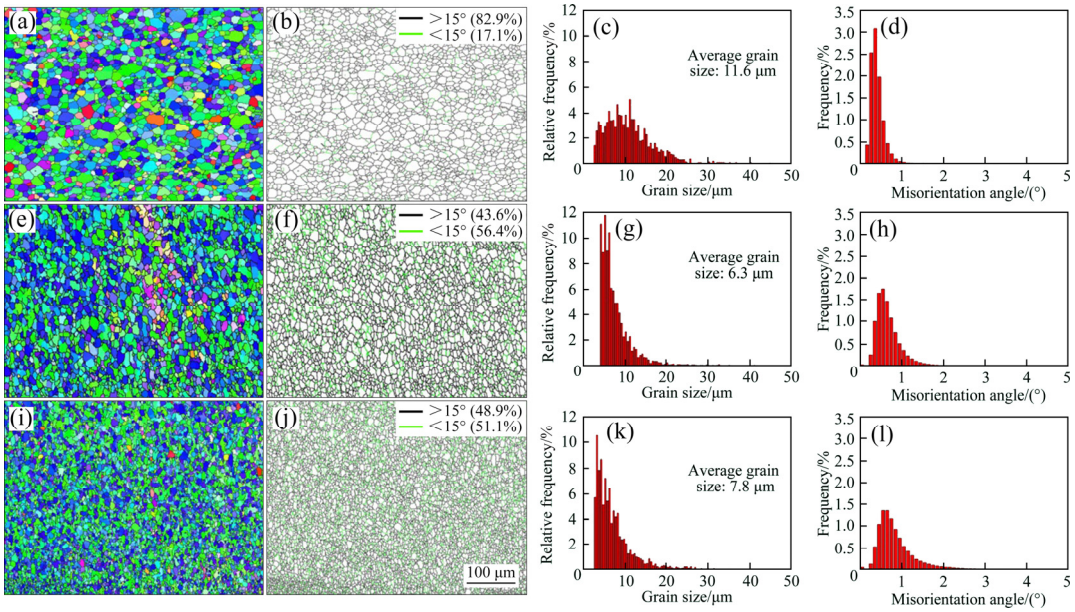

Fig. 2 Microstructure characteristics of BM (a−d) and SZ of 3000-75-1 (e−h) and 3000-75-4 (i−l) samples: (a, e, i) Grain morphology; (b, f, j) Grain boundaries; (c, g, k) Grain size; (d, h, l) Misorientation angle

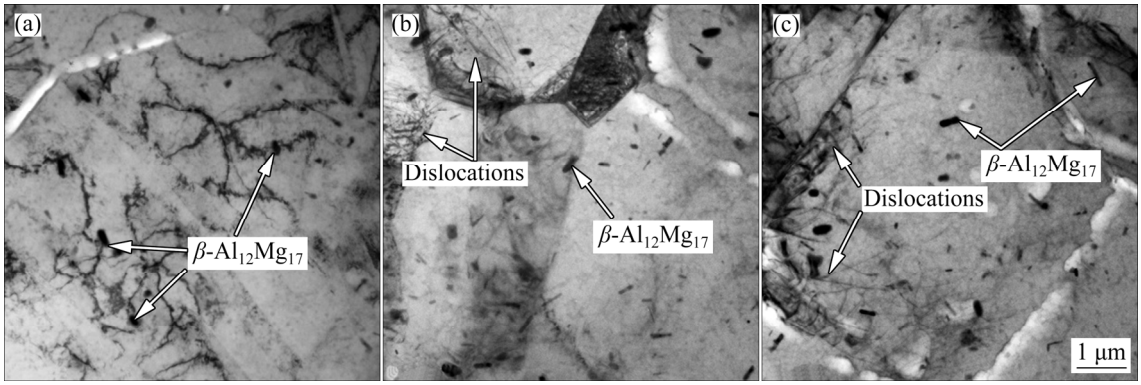

Fig. 3 Precipitate distribution of BM (a) and SZ of 3000-75-1 (b) and 3000-75-4 (c) samples

the SZ prepared by multipass high rotating speed FSP are finer than those in the BM. The average grain size in the SZ prepared by 1-pass and 4-pass FSP are 6.3 and 7.8 μm, 54.3% and 67.2% of the BM (11.6 μm), respectively. The mean grain size in the SZ increases to a certain extent during the subsequent high rotating speed FSP pass. In addition, the number of the low angle grain boundaries (LAGBs) in the SZ is significantly more than that in the BM, whereas the HAGBs is obviously less than that in the BM. Moreover, in addition to the misorientation angle, the number of the LAGBs in the SZ increases with increasing the processing passes, as shown in Figs. 2(f, h, j, l). Compared with the BM, a significant texture is observed in the SZ. The maximum texture intensity in the SZ increases with increasing the processing passes. The maximum texture intensity in the SZ produced by 4-pass high rotating speed FSP is 25.68, which is approximately 2.7 times that of the BM, as shown in Fig. 4.

The distribution characteristics of dislocations and precipitates in the SZ of multipass high rotating speed FSP samples are shown in Figs. 3(b, c). Compared with the BM, a larger number of the β-$Al_{12}Mg_{17}$ precipitates in the SZ are observed. In addition to the increase in size, the distributions of the β-$Al_{12}Mg_{17}$ precipitates also become more uniform with increasing the processing passes. However, the dislocation density in the SZ prepared using 4-pass FSP is lower than that in the 1-pass FSP. It is also clear that the grain size in the SZ

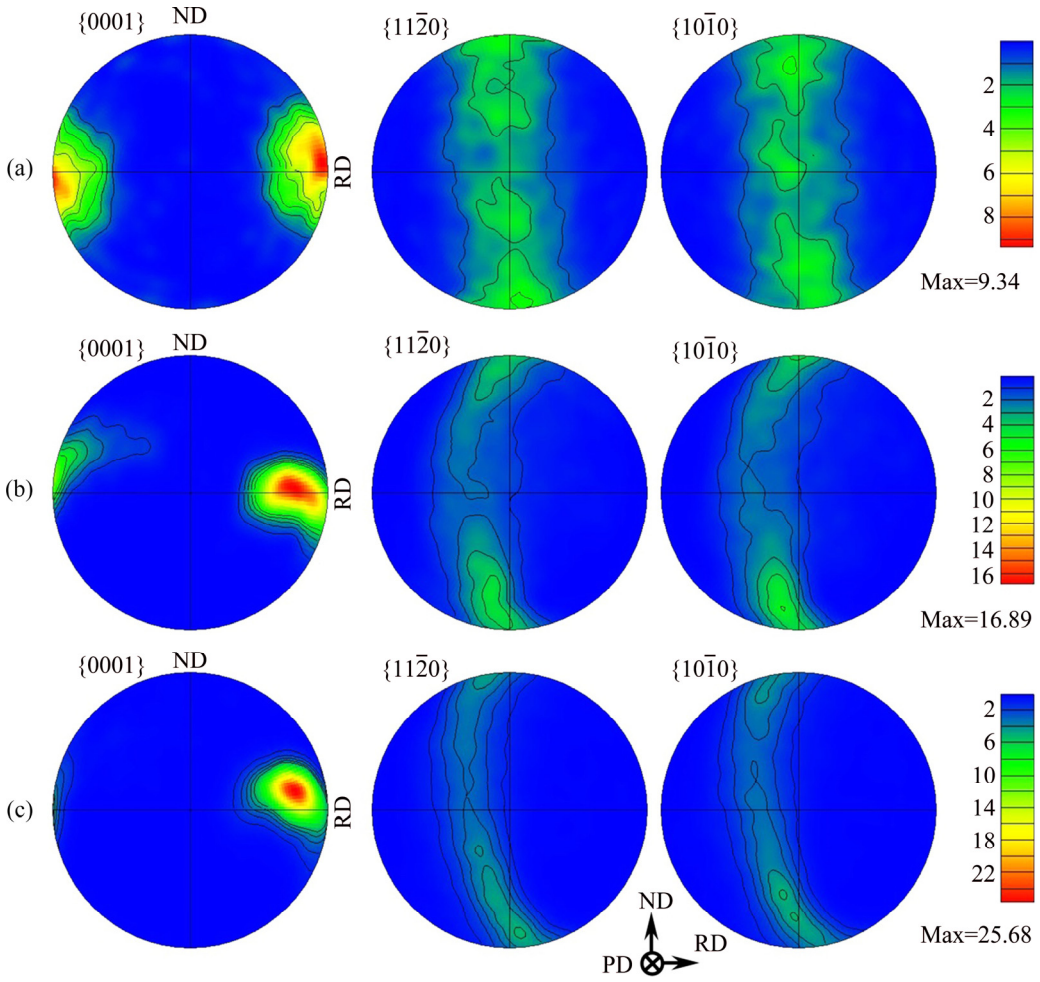

Fig. 4 Pole figures of BM (a) and SZ of 3000-75-1 (b) and 3000-75-4 (c) samples

produced using 1-pass FSP is smaller than that using the 4-pass FSP.

It is well known that magnesium alloys have less SFE than aluminum alloys [22]. This means that grain refinement in magnesium alloys can be easily obtained by dynamic recrystallization (DRX) caused by high temperature and strain rate during thermoplastic processing. This phenomenon has been ascertained in the Mg−Al−Zn magnesium alloy during hot deformation [23]. In the process of high rotating speed FSP, a large number of dislocations in the SZ rapidly initiate and multiply due to large thermal cycle and severe plastic deformation. As a result, a large number of high density dislocations and dislocation walls in the SZ are produced at grain boundaries or large precipitates by slipping and climbing. The high density dislocations and dislocation walls gradually transform into subgrain boundaries by continuously preventing and absorbing dislocations. Partial subgrain boundaries, including newly formed and already existing ones, merge and rotate to turn into the HAGBs. As a result, a large number of LAGBs and HAGBs are produced in the SZ due to DRX. In addition, a large number of β-$Al_{12}Mg_{17}$ precipitates dissolve into the α-Mg to produce massive supersaturated and metastable solid solutions in the SZ due to high temperature and severe plastic deformation in the heating stage. In the subsequent cooling stage, a large number of β-$Al_{12}Mg_{17}$ precipitates reprecipitate from the supersaturated and metastable solid solution. Moreover, the more severe plastic deformation and thermal cycle the SZ suffers, the more complete DRX the SZ experiences. In this way, more HAGBs are produced in the SZ. In addition, more supersaturated and metastable solid solutions are also produced in the SZ due to the higher temperature and severer plastic deformation, and then more precipitates reprecipitate in this region again. In this study, the

rotating speed applied in the FSP is higher than that of the conventional rotating speed. As a result, the temperature in the SZ is higher than that of the conventional rotating speed. MIRONOV et al [24] demonstrated that the welding temperature increased with increasing the rotating speed in the FSW of AZ31 alloy. When the rotating speed is 3000 r/min, the maximum welding temperature is ~0.85T_m (where T_m is the melting point of the AZ31 alloy). This welding temperature is much higher than the recrystallization temperature of the magnesium alloy (205 °C) [25]. The SZ experiences severer plastic deformation due to higher processing temperature. As a result, a larger number of LAGBs and HAGBs in the SZ are produced due to more complete DRX caused by higher processing temperature and severer plastic deformation. In addition, the higher processing temperature and severer plastic deformation also make the orientation of grain rotation and growth stronger, and eventually a stronger texture and larger misorientation angles are produced in this region, as shown in Figs. 2(h, l) and 4. A larger number of β-$Al_{12}Mg_{17}$ precipitates with homogeneous distributions are also produced due to the higher processing temperature and severer plastic deformation. During subsequent passes in multipass high rotating speed FSP, the processing temperature is higher than that in the previous pass due to the accumulation of the previous processing heat, resulting in severer plastic deformation in the processed zone. As a result, a larger number of HAGBs, stronger texture, larger grain sizes and misorientation angles, and more homogeneous distributions of β-$Al_{12}Mg_{17}$ precipitates are produced in the SZ of the 3000-75-4 sample, as shown in Figs. 2−4. It is also found that the fine grains produced at the former FSP process were coarsened during the subsequent passes of FSP [17].

3.2 Corrosion resistance

Figure 5 shows potentiodynamic polarization and Nyquist curves of the BM and SZ prepared by multipass high rotating speed FSP after 30 min of immersion in 3.5 wt.% NaCl aqueous solution. The method of extrapolating the cathodic Tafel region is used to calculate the corrosion potential and corrosion current of the BM and SZ [26], as presented in Table 1. According to the corrosion test results, the corrosion potentials of the BM, 3000-75-1, 3000-75-2 and 3000-75-4 samples are −1.563, −1.270, −1.310, and −1.188 V, respectively. It is implied that the corrosion potential of the SZ prepared for multipass high rotating speed FSP tends to shift to a noble direction. In addition, the corrosion current of all the SZ samples (8.57×10^{-5} A of 3000-75-1, 7.48×10^{-5} A of 3000-75-2 and 5.47×10^{-5} A of 3000-75-4) are less than that of the BM (1.55×10^{-4} A). Generally,

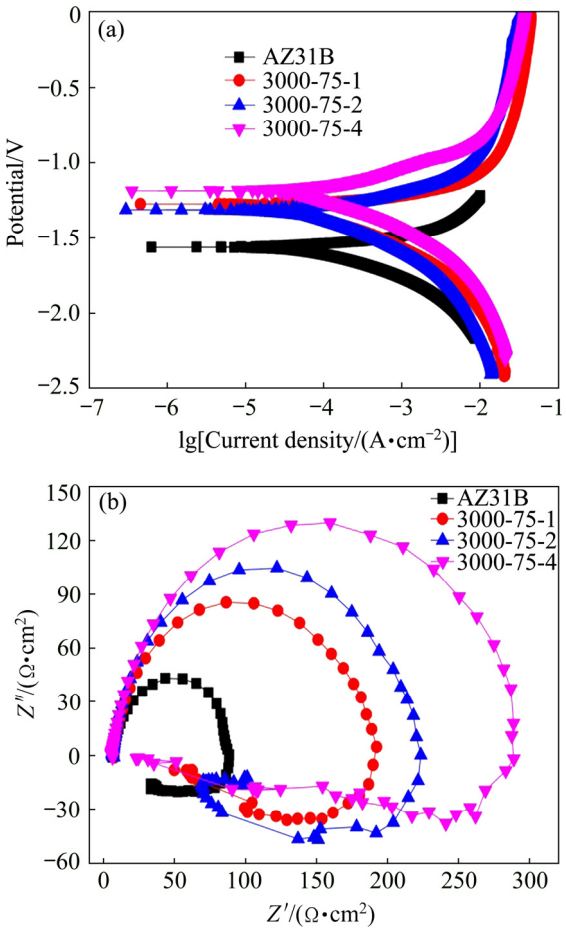

Fig. 5 Potentiodynamic polarization (a) and Nyquist (b) curves of BM and SZ of multipass FSP sample

Table 1 Electrochemical parameters of potentiodynamic polarization curves of BM and SZ calculated by cathodic Tafel extrapolation

Sample	Self-corrosion potential/V	Self-corrosion current/A
AZ31	−1.563	1.55×10^{-4}
3000-75-1	−1.270	8.57×10^{-5}
3000-75-2	−1.310	7.48×10^{-5}
3000-75-4	−1.188	5.47×10^{-5}

the corrosion potential is used to evaluate the initial degree of corrosion, while the corrosion current is applied to ascertaining the corrosion rate at the corrosion potential by Faraday law. According to the test results of potentiodynamic polarization curves, the BM has the worst corrosion resistance. The results have been further determined using an electrochemical impedance spectroscopy, as shown in Fig. 5(b). The diameter of capacitive loop on Nyquist curves is associated with the charge transfer resistance of a working electrode. The corrosion rate of the working electrode decreases as the diameter increases [27]. The Nyquist curves show that the BM has the smallest diameter, indicating that it has the worst corrosion resistance. It is also presented that the corrosion performance of the SZ is gradually enhanced with increasing the processing passes. This means that multipass high rotating speed FSP technology has an obvious effect on improving the corrosion performance of the AZ31 alloy.

Figure 6 presents the corrosion morphologies on the surface of the BM and SZ prepared by multipass high rotating speed FSP. The corrosion damage area and corrosion pits on the surface of the BM are much larger than those of the SZ, which demonstrates that the BM has experienced severer corrosion damage, as shown in Figs. 6(a, d). The corrosion damage area and corrosion pits on the surface of the SZ prepared for 3000-75-1 sample is relatively smaller than those on the BM, indicating that there is less corrosion damage in this sample, as shown in Figs. 6(b, e). The smallest corrosion damage area and shallowest corrosion pits are observed on the surface of the SZ prepared for 3000-75-4 sample, indicating that the least corrosion attack occurred in this sample, as shown in Figs. 6(c, f). The energy dispersive spectrometry (EDS) test results on the corrosion surface of the samples are shown in Fig. 7. The EDS results indicate that there is a large amount of oxygen in the corrosion products. This illustrates that the oxygen is involved in the corrosion attack of magnesium alloy.

It is well known that the AZ31 alloy can exhibit excellent corrosion resistance when it is exposed to dry air. When the AZ31 alloy is exposed to moist atmosphere, the corrosion behavior occurs due to electrochemical reaction. The electrochemical reaction consists of a cathode reaction and an anode reaction. The total corrosion reaction equation is expressed as

$$Mg^{2+}+2OH^{-}\rightarrow Mg(OH)_2 \text{ (corrosion product)} \quad (1)$$

It can be seen from the above equation that magnesium hydroxide can be produced on the bare surface of AZ31 alloy after electrochemical reaction. The magnesium hydroxide film does not effectively protect the magnesium alloy in the sodium chloride solution and is destroyed by the chloride ions. A soluble magnesium salt is formed through the following equation:

$$Mg^{2+}+2Cl^{-}\rightarrow MgCl_2+2e \text{ (corrosion product)} \quad (2)$$

The $MgCl_2$ breaks down the $Mg(OH)_2$ film, and the re-exposed AZ31 alloy continues to be corroded.

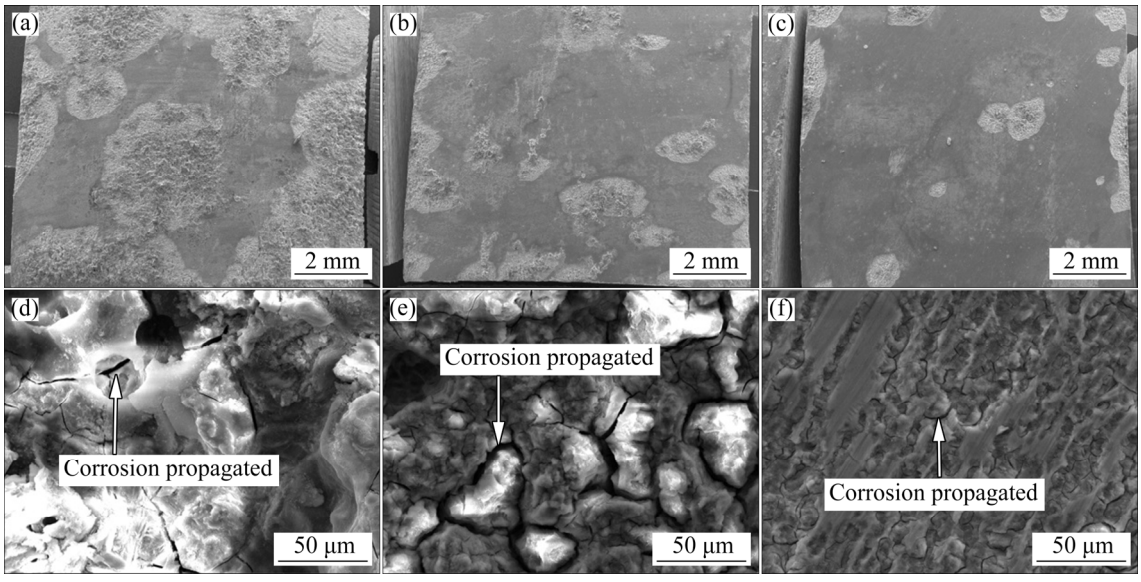

Fig. 6 Corrosion morphologies on surface of BM (a, d) and SZ of 3000-75-1 (b, e) and 3000-75-4 (c, f) samples

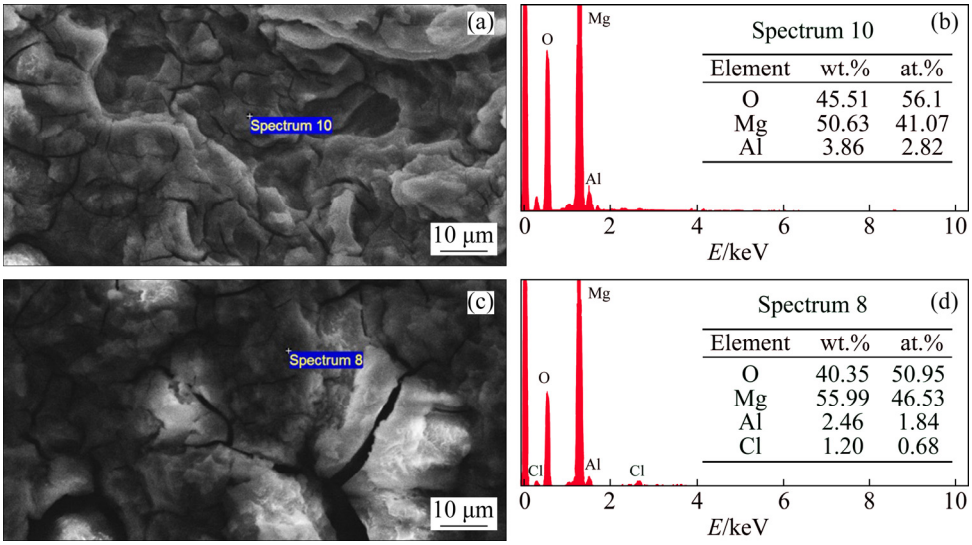

Fig. 7 EDS results on corrosion surface of BM (a, b) and SZ of 3000-75-4 sample (c, d)

Magnesium alloy is sensitive to corrosion at precipitate interface and grain boundary. Once the corrosion occurs, it progresses and expands rapidly along the grain boundary and precipitate interface. For fine grain structures, it is not easy to further corrode along the grain boundary due to the barrier effect of the grain boundary [28]. However, unlike fine grain structure, since the grain boundary hindrance is wear, the coarse grain structure is more easily corroded along the grain boundary. As a result, it is easy to form a large corrosion pit on the magnesium alloy surface. In this study, the mean grain size in the SZ prepared by multipass high rotating speed FSP is smaller than that in the BM. Therefore, the SZ exhibits better corrosion resistance than the BM. However, although the mean grain size in the SZ of 3000-75-4 sample is larger than that of the 3000-75-1 sample, it exhibits better corrosion resistance. This indicates that the grain size is not the most important factor affecting the corrosion resistance of AZ31 alloy. SONG and ATRENS [29] found that the size and distribution characteristics of β-$Al_{12}Mg_{17}$ precipitates were the main factors affecting the corrosion performance of AZ31 alloy, followed by the grain size. The β-$Al_{12}Mg_{17}$ precipitates with proper size and network or dispersive distribution have an obvious effect on improving the corrosion resistance of the AZ31 alloy. In the current work, the distributions of the β-$Al_{12}Mg_{17}$ precipitates in 3000-75-4 sample are more homogeneous and dispersive than those in 3000-75-1 sample, resulting in the fact that the 3000-75-4 exhibits a better corrosion resistance. The corrosion test results indicate that multipass high rotating speed FSP technology can effectively enhance the corrosion resistance of AZ31 alloy.

3.3 Microhardness and tensile properties

Microhardness distributions and mechanical properties of the BM and SZ prepared by multipass high rotating speed FSP are shown in Fig. 8. The tensile properties of the BM and SZ are summarized in Table 2. The average microhardness values of the SZ of 3000-75-1 and 3000-75-4 samples are ~65.1 HV and ~62.5 HV, respectively, which are slightly larger than the microhardness of the AZ31 alloy (~61.5 HV). However, the mean microhardness value of the SZ decreases with increasing the processing passes.

The tensile tests show that the ultimate tensile strength (UTS) of the samples produced using multipass high rotating speed FSP is basically the same as that of the BM except that the yield strength (YS) is slightly improved. The UTS of the SZ ranges from 240.0 to 253.3 MPa, while the YS varies from 129.2 to 132.6 MPa. The elongation (EL) of the SZ is significantly reduced compared to that of the BM. Compared with the 3000-75-1 sample, the tensile properties of the 3000-75-4 sample are slightly reduced, as shown in Fig. 8(b).

Figure 9 presents details of the fracture surfaces of the BM and SZ prepared by multipass high rotating speed FSP after tensile test. The ductile fracture occurs on the surface of the BM, characterized by a large number of dimples and tearing ridges, as shown in Fig. 9(a). The ductile

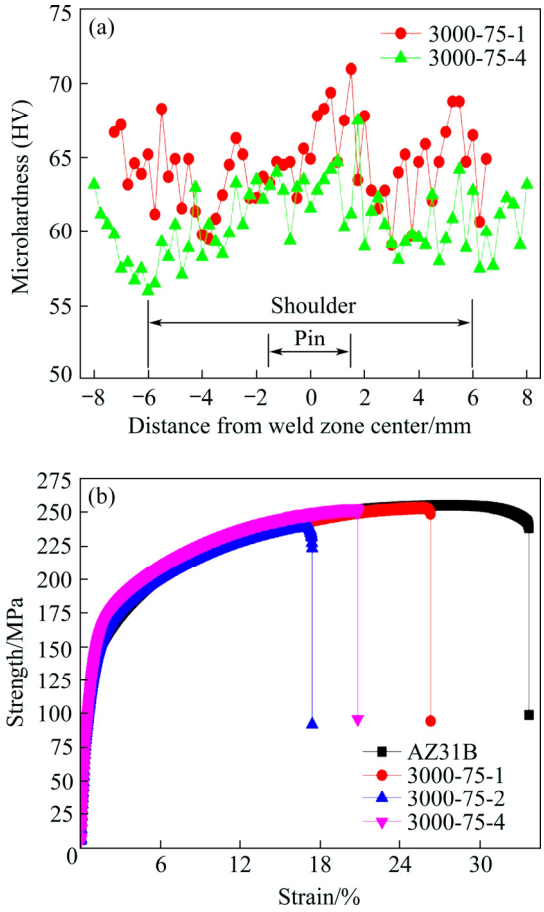

Fig. 8 Microhardness distributions (a) and tensile properties (b) of BM and SZ of multipass FSP samples

Table 2 Tensile properties of BM and SZ of multipass FSP samples

Sample	UTS/MPa	YS/MPa	Elongation/%
AZ31	253.4	127.8	33.7
3000-75-1	253.3	132.6	26.3
3000-75-2	240.0	129.2	17.4
3000-75-4	253.1	130.9	20.8

and brittle fracture occurs on the surface of the 3000-75-1 sample, which exhibits a large number of dimples and cleavage planes, as shown in Fig. 9(b). A large number of shearing lips on the fracture surface of the 3000-75-4 sample indicate that brittle fracture occurs, as shown in Fig. 9(c).

The explanations about the slight variation in the tensile strength of the SZ prepared by multipass high rotating speed FSP mainly are focused on the microhardness distributions, different crystal orientation, and dislocation density and residual stress [25,30,31]. High microhardness values and

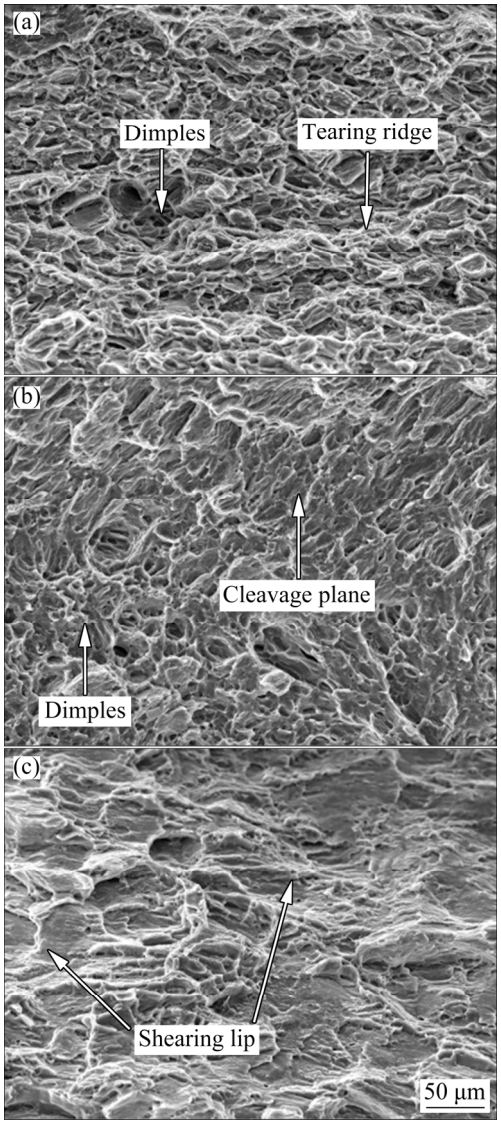

Fig. 9 Fractographs of BM (a) and SZ of 3000-75-1 (b) and 3000-75-4 (c) samples

dislocation density as well as strong texture can effectively improve the tensile strength. In this study, higher microhardness values and more LAGBs as well as stronger texture are produced in the SZ compared to those in the BM, which further compensate the reduction in the tensile strength to some extent caused by the inhomogeneous microstructure. In fact, the tensile specimen of the SZ also contains the unprocessed area at the bottom, resulting in significantly inhomogeneous microstructure from the upper surface to the bottom. As a result, compared with the BM, it is easy to develop stress concentration and initiate microcracks in the adjacent areas with large differences in microstructure, resulting in a significant decrease in elongation. The tensile test results indicate that the

multipass high rotating speed FSP technology has a slight effect on the strength of the AZ31 alloy except for the EL.

4 Conclusions

(1) Multipass high rotating speed FSP can significantly result in a remarkable grain refinement and microstructure homogenization in the SZ of the AZ31 alloy due to complete DRX. The distributions of β-$Al_{12}Mg_{17}$ precipitates can be more dispersed and homogenized in the subsequent processing passes, whereas the grain size increases due to large heat input.

(2) Multipass high rotating speed FSP can significantly improve the corrosion resistance of the SZ mainly due to the diffused and homogenized distributions of the β-$Al_{12}Mg_{17}$ precipitates and refined grains. With the increase of processing passes from 1 to 4, the corrosion potential increases from −1.270 to −1.188 V, while the corrosion current decreases from 8.57×10^{-5} to 5.47×10^{-5} A.

(3) Multipass high rotating speed FSP can improve the average microhardness of the SZ to some extent due to grain refinement and subgrain boundaries. However, in addition to significantly reducing the elongation, the effect of multipass high rotating speed FSP on tensile strength and yield strength of the SZ is slight.

References

[1] ALI Y, QIU D, JIANG B, PAN F S, ZHANG M X. Current research progress in grain refinement of cast magnesium alloys: A review article [J]. Journal of Alloys and Compounds, 2015, 619: 639−651.

[2] LV S L, YANG X, HAO L Y, WU S S, FANG X G, WANG J. Ultrasonic vibration and rheocasting for refinement of Mg−Zn−Y alloy reinforced with LPSO structure [J]. Metals and Materials International, 2018, 24: 1315−1326.

[3] PADHEE C K, MASANTA M, MONDAL A K. Feasibility of Al−TiC coating on AZ91 magnesium alloy by TIG alloying method for tribological application [J]. Transactions of Nonferrous Metals Society of China, 2020, 30: 1550−1559.

[4] PEZZATO L, ANGELINI V, BRUNELLI K, MARTINI C, DABALÀ M. Tribological and corrosion behavior of PEO coatings with graphite nanoparticles on AZ91 and AZ80 magnesium alloys [J]. Transactions of Nonferrous Metals Society of China, 2018, 28: 259−272.

[5] LUO Xian, TAN Qi-yang, MO Ning, YIN Yu, YANG Yan-qing, ZHUANG Wyman, ZHANG Ming-xing. Effect of deep surface rolling on microstructure and properties of AZ91 magnesium alloy [J]. Transactions of Nonferrous Metals Society of China, 2019, 29: 1424−1429.

[6] ZHU S Q, RINGER S P. On the role of twinning and stacking faults on the crystal plasticity and grain refinement in magnesium alloys [J]. Acta Materialia, 2018, 144: 365−375.

[7] DAREINI M, JABBARI A H, SEDIGHI M. Effect of nano-sized Al_2O_3 reinforcing particles on uniaxial and high cycle fatigue behaviors of hot-forged AZ31B magnesium alloy [J]. Transactions of Nonferrous Metals Society of China, 2020, 30: 1249−1266.

[8] ARGADE G R, PANIGRAHI S K, MISHRA R S. Effects of grain size on the corrosion resistance of wrought magnesium alloys containing neodymium [J]. Corrosion Science, 2012, 58: 145−151.

[9] BARADARANI F, MOSTAFAPOUR A, SHALVANDI M. Effect of ultrasonic assisted friction stir welding on microstructure and mechanical properties of AZ91−C magnesium alloy [J]. Transactions of Nonferrous Metals Society of China, 2019, 29: 2514−2522.

[10] VEDABOURISWARAN G, ARAVINDAN S. Development and characterization studies on magnesium alloy (RZ5) surface metal matrix composites through friction stir processing [J]. Journal of Magnesium and Alloys, 2018, 6: 145−163.

[11] BAGHERI B, ABBASI M, ABDOLLAHZADEH A, MIRSALEHI S E. Effect of second-phase particle size and presence of vibration on AZ91/SiC surface composite layer produced by FSP [J]. Transactions of Nonferrous Metals Society of China, 2020, 30: 905−916.

[12] RAJA A, PANCHOLI V. Effect of friction stir processing on tensile and fracture behaviour of AZ91 alloy [J]. Journal of Materials Processing Technology, 2017, 248: 8−17.

[13] LUO X C, ZHANG D T, CAO G H, QIU C, CHEN D L. High-temperature tensile behavior of AZ61 magnesium plate prepared by multi-pass friction stir processing [J]. Materials Science and Engineering A, 2019, 759: 234−240.

[14] CHAI F, YAN F, WANG W, LU Q C, FANG X. Microstructures and mechanical properties of AZ91 alloys prepared by multi-pass friction stir processing [J]. Journal of Materials Research, 2018, 33: 1789−1796.

[15] LUO X C, ZHANG D T, ZHANG W W, QIU C, CHEN D L. Tensile properties of AZ61 magnesium alloy produced by multi-pass friction stir processing: Effect of sample orientation [J]. Materials Science and Engineering A, 2018, 725: 398−405.

[16] LUO X C, ZHANG D T, CAO G H, QIU C, CHEN D L. Multi-pass submerged friction stir processing of AZ61 magnesium alloy: Strengthening mechanisms and fracture behavior [J]. Journal of Materials Science, 2019, 54: 8640−8654.

[17] VENKATESWARLU G, DEVARAJU D, DAVIDSON M J, KOTIVEERACHARI B, TAGORE G R N. Effect of overlapping ratio on mechanical properties and formability of friction stir processed Mg AZ31B alloy [J]. Materials and Design, 2013, 45: 480−486.

[18] NIA A A, OMIDVAR H, NOURBAKHSH S H. Effects of an overlapping multi-pass friction stir process and rapid cooling on the mechanical properties and microstructure of

AZ31 magnesium alloy [J]. Materials and Design, 2014, 58: 298−304.
[19] LIU D J, SHEN M X, YANG Y C, HU Y, ZHAO L Z. Evaluation of corrosion resistance of multipass friction stir processed AZ31 magnesium alloy [J]. Materials and Corrosion, 2019, 70: 1553−1560.
[20] ZHANG J Y, UPADHYAY P, HOVANSKI Y, FIELD D P. High-speed friction stir welding of AA7075-T6 sheet: Microstructure, mechanical properties, micro-texture, and thermal history [J]. Metallurgical and Materials Transactions A, 2018, 49: 210−222.
[21] HIRAI K, SOMEKAWA H, TAKIGAWA Y, HIGASHI K. Superplastic forging with dynamic recrystallization of Mg−Al−Zn alloys cast by thixo-molding [J]. Scripta Materialia, 2007, 56: 237−240.
[22] WANG Y, CHEN L Q, LIU Z K, MATHAUDHU S N. First-principles calculations of twin-boundary and stacking-fault energies in magnesium [J]. Scripta Materialia, 2010, 62: 646−649.
[23] CHINO Y, KOBATA M, IWASAKI H, MABUCHI M. An investigation of compressive deformation behaviour for AZ91 Mg alloy containing a small volume of liquid [J]. Acta Materialia, 2003, 51: 3309−3318.
[24] MIRONOV S, SATO Y S, KOKAWA H. Influence of welding temperature on material flow during friction stir welding of AZ31 magnesium alloy [J]. Metallurgical and Materials Transactions A, 2019, 50: 2798−2806.
[25] LI W Y, NIU P L, YAN S R, PATEL V, WEN Q. Improving microstructural and tensile properties of AZ31B magnesium alloy joints by stationary shoulder friction stir welding [J]. Journal of Manufacturing Processes, 2019, 37: 159−167.
[26] LI J R, JIANG Q T, SUN H Y, LI Y T. Effect of heat treatment on corrosion behavior of AZ63 magnesium alloy in 3.5 wt.% sodium chloride solution [J]. Corrosion Science, 2016, 111: 288−301.
[27] KING A D, BIRBILIS N, SCULLY J R. Accurate electrochemical measurement of magnesium corrosion rates: A combined impedance, mass-loss and hydrogen collection study [J]. Electrochimica Acta, 2014, 121: 394−406.
[28] JIANG J H, MA A B, SAITO N, SHEN Z X, SONG D, LU F M, NISHIDA Y, YANG D H, LIN P H. Improving corrosion resistance of RE-containing magnesium alloy ZE41A through ECAP [J]. Journal of Rare Earths, 2009, 27: 848−852.
[29] SONG G L, ATRENS A. Corrosion mechanisms of magnesium alloys [J]. Advanced Engineering Materials, 1999, 1: 11−33.
[30] ESPARZA J A, DAVIS W C, TRILLO E A, MURR L E. Friction-stir welding of magnesium alloy AZ31B [J]. Journal of Materials Science Letters, 2002, 21: 917−920.
[31] LI G H, ZHOU L, LUO S F, DONG F B, GUO N. Microstructure and mechanical properties of bobbin tool friction stir welded ZK60 magnesium alloy [J]. Materials Science and Engineering A, 2020, 776: 138953.

多道次高转速搅拌摩擦加工对 AZ31 合金加工区显微组织演变、腐蚀行为和力学性能的影响

刘奋军[1,2]，姬 妍[1,2]，白艳霞[1]

1. 榆林学院 能源工程学院，榆林 719000；
2. 榆林学院 榆林市金属基复合材料与再制造技术重点实验室，榆林 719000

摘 要：采用 EBSD、TEM、SEM、电化学工作站和电子万能实验机研究多道次高转速搅拌摩擦加工对 AZ31 合金加工区显微组织演变、腐蚀行为和力学性能的影响。结果表明，加工区平均晶粒尺寸显著细化。增加加工道次，加工区晶粒粗化，而 β-$Al_{12}Mg_{17}$ 析出相增多并变得更加连续和均匀。与 AZ31 合金相比，加工区拉伸性能变化轻微，但是耐腐蚀性能得到显著提升。4 道次高转速搅拌摩擦加工制备的合金其加工区自腐蚀电位由−1.56 V 增加至−1.19 V，而自腐蚀电流从 1.55×10^{-4} A 减小至 5.47×10^{-5} A。

关键词：AZ31 合金；高转速；多道次搅拌摩擦加工；显微组织演变；耐腐蚀性；力学性能

(Edited by Bing YANG)